American Mineralogist, Volume 110, pages 767–775, 2025

Episodic magmatism contributes to sub-seafloor copper mineralization: Insights from textures and geochemistry of zoned pyrite in the Ashele VMS deposit

Bing Xiao[1,2,3,4], Huayong Chen[1,2,3,*], Yuzhou Feng[1,4], and Yuanming Pan[4,†]

[1]State Key Laboratory of Deep Earth Processes and Resources, Guangzhou Institute of Geochemistry, Chinese Academy of Sciences, Guangzhou 510640, China
[2]University of Chinese Academy of Sciences, Beijing 100049, China
[3]Guangdong Provincial Key Laboratory of Mineral Physics and Materials, Guangzhou 510640, China
[4]Department of Geological Sciences, University of Saskatchewan, Saskatoon, Saskatoon S7N 5E2, Canada

Abstract

Prolonged and episodic magmatic-hydrothermal processes have been proposed to be important in forming large-tonnage Cu volcanogenic massive sulfide (VMS) deposits but are difficult to document and remain poorly understood in ancient VMS systems. In this study, we combine textural evidence and in situ analysis of sulfur isotopic composition with trace elements of pyrite from the well-preserved, large-tonnage Ashele VMS deposit (Central Asian Orogenic Belt, NW China) to elucidate the origin of the ore-forming materials and controlling factors of VMS deposits. The distribution of hydrothermal alteration and mineralization allows the Ashele deposit to be divided into five zones: massive sulfide, quartz-pyrite, chlorite-chalcopyrite-quartz-pyrite, quartz-chlorite-sericite-pyrite, and quartz-sericite-pyrite zones. Cu mineralization is mainly hosed in the massive sulfide and chlorite-chalcopyrite-quartz-pyrite zones. Three texturally and compositionally distinct types of pyrite from the Cu mineralization zones have been recognized. The first type of growth zones with high Cu, As, and volatile elements (e.g., Hg and Tl) concentrations and negative $\delta^{34}S$ values (−7.83‰ to −0.35‰) are observed in pyrite grains from the massive sulfide zone most likely formed from the input of magmatic volatiles degassed from the underlying magmatic systems. The second type of Cu-As-rich growth zones in pyrite grains from the chlorite-chalcopyrite-pyrite zone is not enriched in volatile elements and has positive $\delta^{34}S$ values (2.59–6.56‰), which are interpreted to have precipitated during fluid boiling. The third type of growth zone, without Cu-As enrichment but having positive $\delta^{34}S$ values (0.30–9.76‰) in pyrite grains from both mineralization zones, was probably formed without boiling or magmatic volatile input. Our results suggest that multi-stage magmatic degassing or fluid boiling accompanied by Cu precipitation recorded in individual pyrite grains can reveal episodic magmatic-hydrothermal activity, which is an essential factor in forming large-tonnage VMS deposits.

Keywords: Pyrite chemistry, in situ analysis, episodic magmatic activity, VMS deposit

Introduction

Volcanogenic massive sulfide (VMS) deposits, formed at mid-ocean ridges, as well as intra-oceanic arc and back-arc basin settings, supply significant Cu, Zn, Pb, Au, Ag, and other byproduct metals (Large 1992; Franklin et al. 2005). Understanding the processes that lead to the formation of these deposits is key to the exploration and sustainable production of these important resources. It is generally recognized that VMS deposits formed through the leaching of metals from underlying volcanic host rocks by heated seawater (i.e., the seawater model, Richardson et al. 1987; Seyfried and Ding 1993; Franklin et al. 2005; Jowitt et al. 2012; Patten et al. 2017). However, other studies argued that magmatic fluids from the underlying magma chamber through magmatic degassing could be the source of metals (i.e., the magmatic fluid model, Yang and Scott 1996; de Ronde et al. 2011; Brueckner et al. 2014; Martin et al. 2020; Falkenberg et al. 2022). In addition, numerical simulations have indicated that the formation of a large-tonnage, Cu-rich VMS deposits may require a long-lived hydrothermal system related to the underlying magma chamber (e.g., >35 kyr at the Matsumine deposit; Cathles 1983; Barrie et al. 1999; Schardt and Large 2009). These simulations are based on the assumption that the mineralization processes of VMS are continuous. However, recent in situ analyses of Sr isotope ratios and trace element contents of zoned epidote in the alteration pipe of Cyprus VMS deposits indicated that episodic fluxing of magmatic fluids was involved in the alteration and mineralization processes of these VMS systems (Fox et al. 2020). To advance our understanding of the controls on the formation of VMS deposits, it is critical to further evaluate the source of metals (i.e., seawater vs. magmatic fluids) and the evolution of mineralizing fluids and associated magmatism (i.e., episodic or continuous).

In addition to the presence of an ore-forming fluid, an efficient trigger is required to precipitate ore minerals. For the seawater model, metal precipitation is likely controlled by changes in fluid temperature and pH caused by mixing with seawater (Franklin et al. 2005; Hannington 2014). While for the magmatic fluid model, fluid boiling and magmatic degassing may have resulted in abrupt physicochemical changes in the hydrothermal

* Corresponding author E-mail: huayongchen@gig.ac.cn
† Orcid https://orcid.org/0000-0002-9195-3776

0003-004X/25/0005–767$05.00/DOI: https://doi.org/10.2138/am-2023-9250

fluids and rapid metal precipitation (Tardani et al. 2017; Román et al. 2019; Falkenberg et al. 2021; Keith et al. 2022). Hence, it is crucial to precisely determine the specific processes for metal precipitation and their contributions to Cu mineralization during continuous or episodic magmatic-hydrothermal activities in VMS systems.

Pyrite is ubiquitous in VMS systems, can incorporate a wide variety of trace elements, and possesses distinct isotopic fingerprints. The trace-element compositions of pyrite are controlled by the physicochemical conditions of the hydrothermal fluid, making pyrite an excellent tracer mineral for fluid evolution during mineralizing processes (Large et al. 2009; Reich et al. 2013; Brueckner et al. 2016; Ishida et al. 2022; Zhang et al. 2022). Similarly, in situ sulfur isotope analyses of pyrite in VMS deposits can be used to discriminate contributions from isotopically distinct reservoirs of sulfur in hydrothermal fluids, such as sulfur leached from oceanic crust (~0‰) (Ohmoto 1972), seawater sulfate (4–33‰) (Brueckner et al. 2015), and SO_2 degassing from shallow magma chambers (<0‰) (Herzig et al. 1998). In this study, we made detailed documentation of pyrite textures in the well-preserved, large-tonnage Ashele VMS deposit from the Central Asian Orogenic Belt and performed in situ analyses of sulfur isotopes and trace elements in pyrite, aiming to identify multiple stages of mineralization/magmatism and shed new light on the critical factors controlling mineralization in large-tonnage VMS systems.

Deposit Geology

The Early-to-Middle Devonian Ashele deposit is the largest known VMS Cu-Zn deposit in the Chinese Altay Orogen (Fig. 1), containing significant Cu (1.08 Mt. at 2.46%), Zn (0.43 Mt. at 0.41%), and Au (27.2 t at 0.36 g/t) (Zheng et al. 2016). Detailed geological descriptions of the Ashele Cu-Zn deposit are available in Wan et al. (2010), Zheng et al. (2016), Yang et al. (2018), and Xiao et al. (2024). Mineralization and hydrothermal alteration are generally hosted by the first and second sub-members of the second unit in the Ashele Formation. The first sub-member comprises basalt, tuff, breccia tuff, rhyolite, and limestone, while the second sub-member consists of tuff, sedimentary tuff, breccia tuff, barite, and limestone (Zheng et al. 2016). Hydrothermal alteration and mineralization zonation at the Ashele deposit are well developed in the volcanic tuff that makes up the hanging wall of the deposit (Fig. 2a).

The Ashele deposit can be divided into five zones (outwards from the mineralization center), i.e., massive sulfide, quartz-pyrite, chlorite-quartz-chalcopyrite-pyrite, quartz-chlorite-sericite-pyrite, and quartz-sericite-pyrite zones (Fig. 2b) (Xiao et al. 2024), with most Cu mineralization in the massive sulfide and chlorite-quartz-chalcopyrite-pyrite zones. The massive sulfide zone is composed mainly of colloidal and euhedral pyrite, with minor chalcopyrite, quartz, sphalerite, sericite, chlorite, barite, and tourmaline (Fig. 2c). The chlorite-quartz-chalcopyrite-pyrite zone is characterized by intense chlorite alteration with

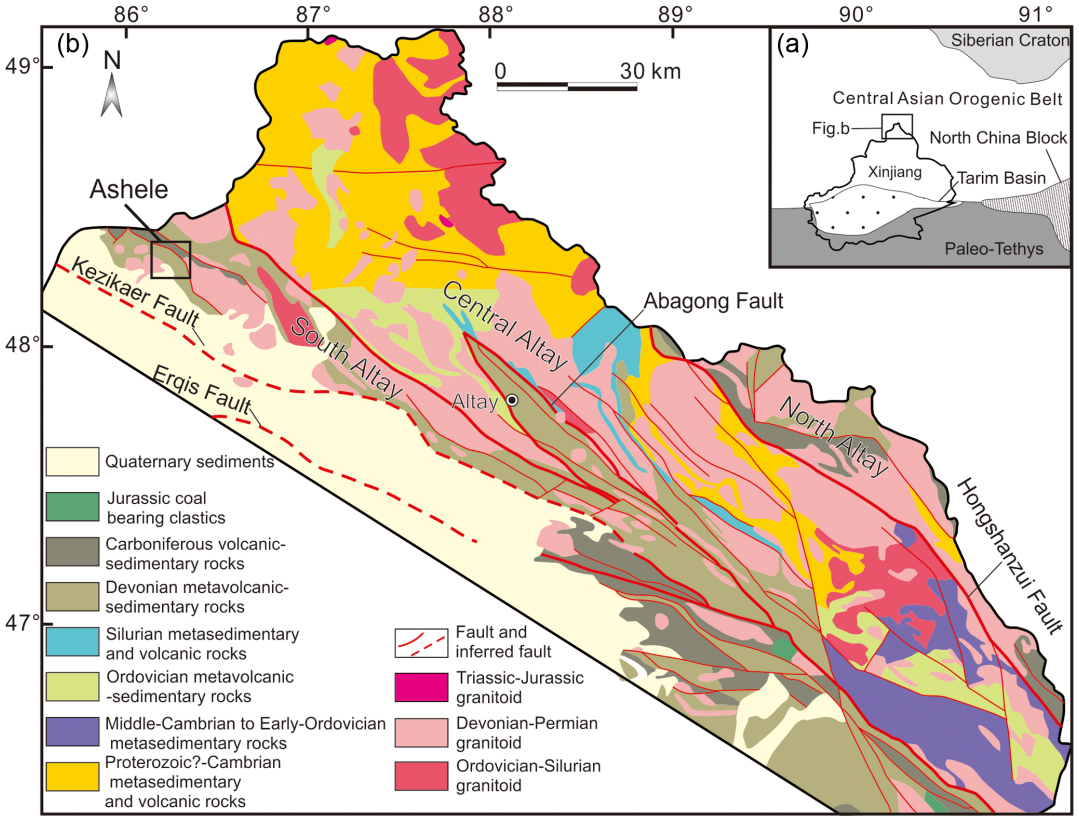

Figure 1. Simplified regional geological map of the Altay Mountains, Xinjiang (after Yang et al. 2018), showing the location of the Ashele VMS deposit. (Color online.)

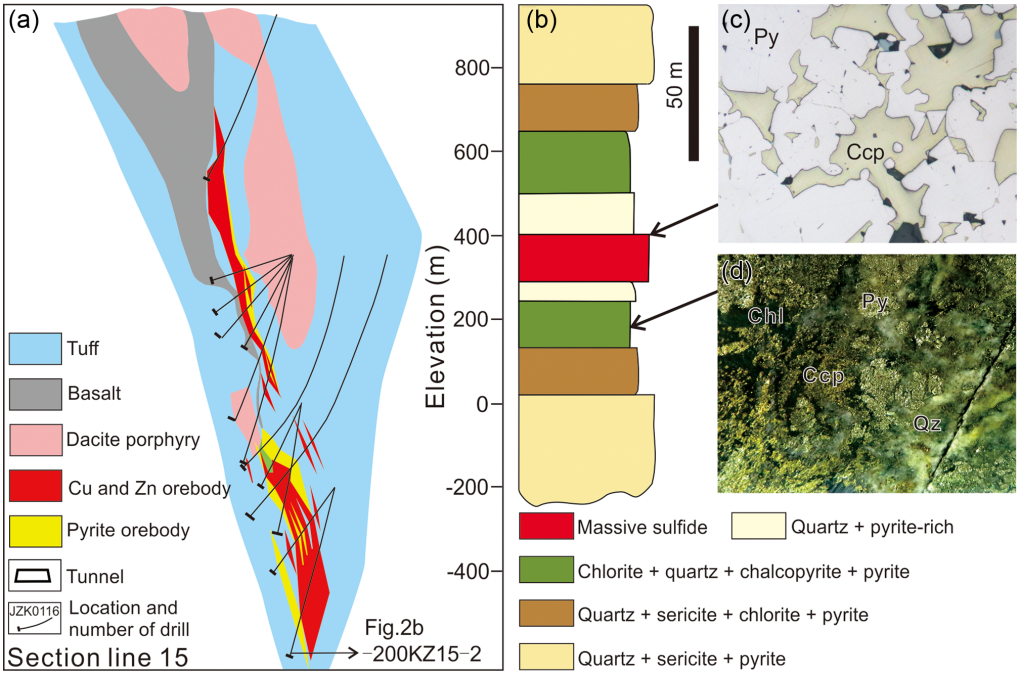

Figure 2. (**a**) Cross sections along the Exploration Line 15; (**b**) simplified drill log for the -200KZ15-2 hole; (**c**) photomicrograph of a representative sample from the massive sulfide zone; (**d**) photomicrograph of a representative sample from the chlorite-quartz-chalcopyrite-pyrite zone of the Ashele VMS deposit. (Color online.)

disseminated chalcopyrite (Fig. 2d) overprinting earlier quartz and pyrite, which represents a stringer-zone orebody in the Ashele VMS deposit (Xiao et al. 2024).

Sampling and Analytical Methods

In this study, a total of 10 representative samples, 5 from the massive sulfide zone and 5 from the chlorite-quartz-chalcopyrite-pyrite zone, were investigated. Polished thin sections of these samples were first examined using transmitted and reflected light microscopy and then backscattered electron (BSE) imaging to characterize textural relationships. Representative samples were then analyzed in situ by secondary ion mass spectrometry (SIMS) and laser-ablation inductively coupled plasma-mass spectrometry (LA-ICP-MS) to determine trace-element and sulfur isotope compositional characteristics. The locations of samples investigated in this study are listed in the Online Materials[1] Appendix I.

Prior to the BSE imaging, selected polished thin sections were etched by sodium hypochlorite NaOCl (~5%; 15 s) and then photographed under a reflected-light microscope to reveal microstructures such as zoning, microfractures, and grain boundaries. The etching of pyrite also enabled the selection of areas free of mineral inclusions and microfractures for SIMS and LA-ICP-MS analysis. The BSE imaging was carried out on polished thin sections using a TESCAN MIRA3 field-emission scanning electron microprobe (FE-SEM) at the Testing Center, Tuoyan Analytical Technology Co. Ltd. (Guangzhou, China). After the samples were carbon-coated, SEM images were acquired at an acceleration voltage of 20 kV and a beam current of 15 nA.

The SIMS analysis of pyrite was conducted using a Cameca IMS1280-HR at the Guangzhou Institute of Geochemistry, Chinese Academy of Sciences. The following conditions were used for the measurements of all standards and samples: 20 keV total impact energy, ~2.0 nA beam current, and 10 µm beam diameter. Prior to SIMS analysis, 20 s of pre-sputtering was applied to remove the Au coating, and a normal-incidence electron gun was used for charge compensation. Isotopes ^{32}S, ^{33}S, and ^{34}S were measured simultaneously by the Cameca IMS 1280-HR multi-collection system and the total analysis time for each spot was about 4 min. The primary standard used was PPP-1 (Gilbert et al. 2014) for pyrite and the in-house sample Py-1 (Maier et al. 2016; Molnár et al. 2016) was used as the secondary pyrite standard. Correction factors of the instrumental bias of $\delta^{34}S$ for pyrite measurements were determined using $\delta^{34}S_{raw}$ values of bracketing analyses of Py-1 ($\delta^{34}S = -0.6‰$ VCDT) as follows: α_{SIMS} (pyrite) = $[1 + \delta^{34}S_{raw}(\text{Py-1})/1000]/1.01604$. The average $\delta^{34}S$ value that we obtained on the standard Py-1 [$-0.6 \pm 0.1‰$ (2σ); n = 10] is consistent with the recommended value [$-0.6 \pm 0.6‰$ (2σ)] (Maier et al. 2016; Molnár et al. 2016). More details can be found in Li et al. (2020). The S isotope data are listed in Online Materials[1] Appendix II, and the corresponding BSE images of the samples for SIMS analysis are given in Online Materials[1] Appendixes III and IV.

Mapping of trace elements in pyrite was made using a NWR 193 nm ArF Excimer laser ablation (LA) system coupled to an iCAP RQ inductively coupled plasma-mass spectrometer (ICP-MS) at the Guangzhou Tuoyan Microregion Testing Center, Guangzhou, China. The ICP-MS was tuned using the NIST 610 standard glass to yield low oxide production rates. A 0.7 L/min He carrier gas was fed into the cup, and the aerosol was subsequently mixed with 0.89 L/min Ar make-up gas. Samples were ablated with an 8 µm diameter circular ablation area, a repetition rate of 10 Hz, and a laser fluence of 3.5 J/cm^2. The laser scan speed was 10 µm/s. The raw isotope data were reduced using the "TRACE ELEMENTS" data reduction scheme (DRS). The DRS runs within the freeware IOLITE package of Paton et al. (2011). In IOLITE, user-defined time intervals are established for the baseline correction procedure to calculate session-wide baseline-corrected values for each isotope. Two silicate standards (NIST 610 and GSE-2G) and one sulfide standard (MASS-1) were analyzed after 5 to 8 unknown sample analyses. All the isotopes were quantified using ^{57}Fe (Fe = 46.6%) as an internal standard. The LA-ICP-MS plot data are listed in Online Materials[1] Appendix V and LA-ICP-MS mapping images in Online Materials[1] Appendixes VI and VII.

Results

Multiple generations of pyrite

Based on petrographic observations, NaOCl etching, BSE imaging, and LA-ICP-MS mapping analyses, complicated zones were recognized in pyrite from the Ashele deposit (Online Materials[1] Appendixes III and IV). For example, pyrite from the massive sulfide zone consists of five growth zones (Fig. 3;

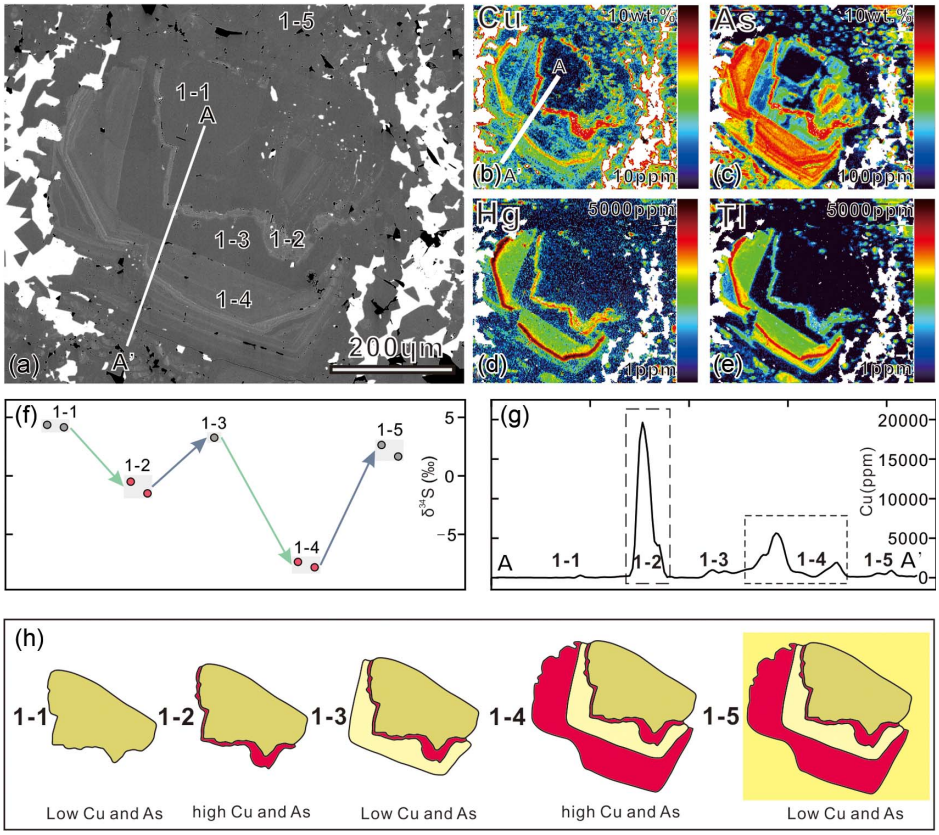

FIGURE 3. (**a**) Backscattered electron image with SIMS analytical spots, (**b**–**e**) LA-ICP-MS element maps, SIMS $\delta^{34}S$ values (**f**) and Cu contents (**g**) of pyrite from the massive sulfide zone, and (**h**) the five-stage growth history inferred from petrographic observations of representative pyrite grains from the massive sulfide zone of the Ashele VMS deposit. The transect of Cu concentrations is extracted from the LA-ICP-MS map data. (Color online.)

Online Materials[1] Appendix IIIa): an inclusion-free core Py1-1, a porous and inclusion-rich Py1-2, a second inclusion-free zone Py1-3, an oscillatory-zoned overgrowth Py1-4, and an outer xenomorphic zone Py1-5. Pyrite from the chlorite-quartz-chalcopyrite-pyrite zone also shows five growth zones (Fig. 4; Online Materials[1] Appendix IVa): a porous and inclusion-rich core Py2-1, porous and inclusion-free zones Py2-2 and Py2-4, and porous zones Py2-3 and Py2-5.

Sulfur isotopes

Figure 5 shows the in situ sulfur isotope compositions of pyrite in the Ashele deposit. Compared with chalcopyrite (0.01–4.15‰ $\delta^{34}S$) (Xiao et al. 2024) and sphalerite (0.40–0.90‰ $\delta^{34}S$) (Yang et al. 2018), pyrite in the Ashele deposit has larger $\delta^{34}S$ variations (−7.83–9.76‰). Combined with our previous S isotope study (Xiao et al. 2024), pyrite grains in the chlorite-quartz-chalcopyrite-pyrite zone have $\delta^{34}S$ values ranging from 1.25 to 9.76‰ with an average of 5.18 ± 0.77‰ (1σ and n = 17). Pyrite grains in the massive sulfide zone have a larger range of $\delta^{34}S$ values ranging from −7.83 to 5.87‰ with an average value of 1.92 ± 0.79‰ (1σ and n = 55).

LA-ICP-MS trace-element spot and mapping analyses

A total of 43 LA-ICP-MS spots and two trace-element mapping analyses were conducted in this study for all pyrite generations identified in the mineralization zones of the Ashele deposit. Combined with chemical etching and BSE images, LA-ICP-MS spot and mapping analyses indicate that the zonal textures of pyrite are mainly expressed by variable As and Cu contents. Zones Py1-1, Py1-3, and Py1-5 from the massive sulfide zone have very low trace element concentrations with positive $\delta^{34}S$ values, whereas Py1-2 and Py1-4 are enriched in Cu, As, Mn, Zn, Se, Mo, Ag, Sb, Te, Hg, Tl, and Pb with negative $\delta^{34}S$ values (Fig. 3). Although pyrite from the chlorite-quartz-chalcopyrite-pyrite zone displays multiple textures, its texturally distinct zones all have positive $\delta^{34}S$ values. Specifically, the porous Py2-1, Py2-3, and Py2-5 have elevated concentrations of Cu, As, Co, Pb, Mn, Bi, Zn, Te, Se, Ag, Te, and In but are poor in Sb, Hg and Tl (Fig. 4). Chalcopyrite is developed around As-Cu enriched growth zones in pyrite grains from both the massive sulfide and chlorite-quartz-chalcopyrite-pyrite zones (Figs. 3 and 4).

DISCUSSION

Source of mineralizing fluids

The overall sulfur isotope composition of pyrite at Ashele ranges from −7.83 to 9.76‰ (Fig. 5), with the largest intra-grain variation from −7.83 to 4.36‰ (Online Materials[1] Appendix III), suggesting that the source of sulfur must have varied significantly as the pyrite crystals grew. The positive values of sulfur isotope (1.65–6.56‰, avg. 4.45‰, n = 69) found in pyrite growth zones from the massive sulfide and chlorite-quartz-chalcopyrite-pyrite

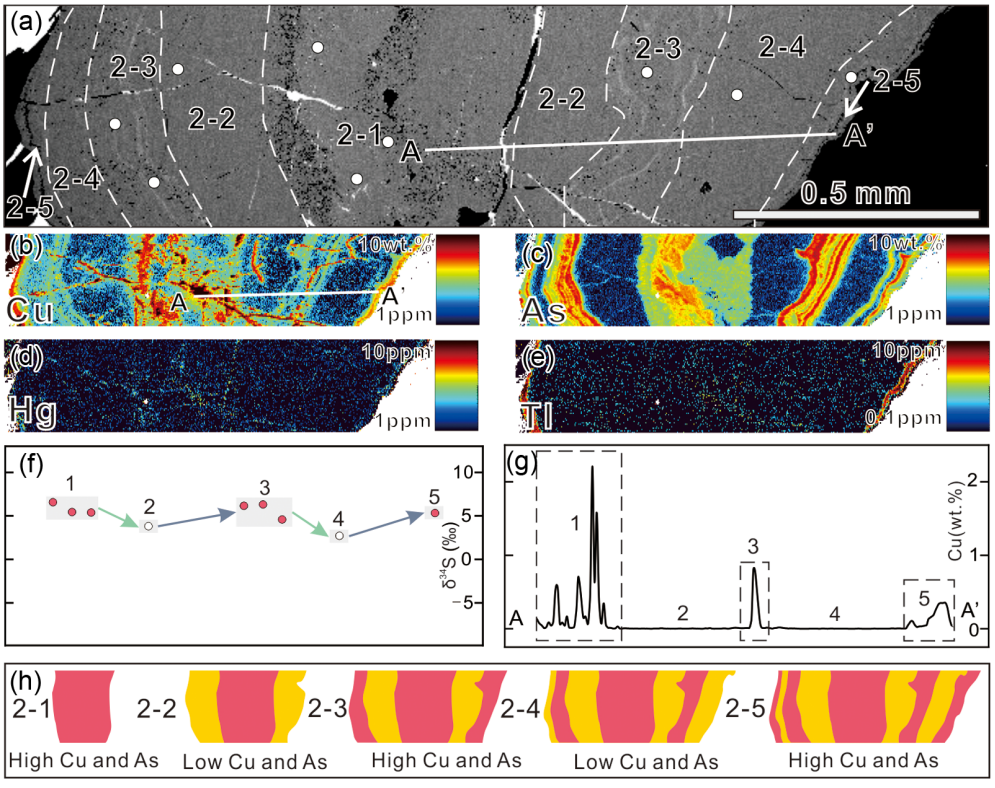

Figure 4. (**a**) Backscattered electron image with SIMS analytical spots, (**b**–**e**) LA-ICP-MS element maps, SIMS $\delta^{34}S$ values (**f**) and Cu contents (**g**), and (**h**) the five-stage growth history inferred from petrographic observations of a representative pyrite grain from the chlorite-quartz-chalcopyrite-pyrite zone of the Ashele VMS deposit. The transect of Cu concentrations is extracted from the LA-ICP-MS map data. (Color online.)

zones suggest that sulfur in these growth zones is mainly derived from leaching of volcanic rocks (~0‰) (Ohmoto 1972) and thermochemical sulfate reduction (TSR) of Devonian seawater (18.5‰) (Holser 1977). However, these processes cannot account for the negative $\delta^{34}S$ values (−7.83‰ to −0.50‰, n = 11, avg. −4.30‰) of pyrite growth zones from the massive sulfide zone. The absence of any framboidal pyrite and high formation temperatures [>200 °C, according to fluid inclusion analyses of Yang et al. (2018)] also exclude the involvement of low-temperature (generally <100 °C) seawater sulfates via bacterial sulfate reduction (BSR) (Nozaki et al. 2020). In addition, these pyrite growth zones with negative $\delta^{34}S$ values have high $Se/S \times 10^6$ ratios (>500), also indicating magmatic volatile influxes (Martin et al. 2020). Therefore, we suggest that the negative $\delta^{34}S$ values in pyrite from the massive sulfide zone most likely recorded degassing of an underlying magma body where disproportionation of magmatic volatile-derived SO_2 produced ^{34}S-enriched H_2SO_4 and ^{34}S-depleted H_2S (Herzig et al. 1998).

Episodic Cu mineralization recorded by zoned pyrite

The input of magmatic volatiles can lead to a significant increase of the Cu, As, Te, Se, Sb, Pb, Tl, and Hg concentrations in hydrothermal fluids (Layton-Matthews et al. 2013; Wohlgemuth-Ueberwasser et al. 2015; Berkenbosch et al. 2019). The correlation between negative $\delta^{34}S$ values and trace-element abundances (Cu, As, Te, Se, Sb, Pb, Tl, and Hg; Online Materials[1] Appendix VI) in certain growth zones of pyrite indicate that magmatic volatiles (Hg and Tl) could play an important role in mineralization in the massive sulfide zone, which is consistent with high $^3He/^4He$ ratios (0.14 to 0.26 R/Ra) of fluid inclusions in pyrite (Yang et al. 2018). It is important to note that a single pyrite grain, only a few hundred micrometers in diameter, in the massive sulfide zone records at least two pulses of magmatic volatiles (Fig. 3), indicating that multiple magmatic volatile influxes occurred as episodic releases into the overlying hydrothermal

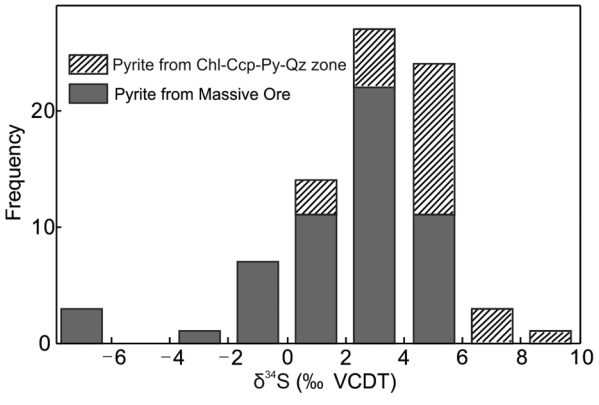

Figure 5. Histogram of $\delta^{34}S$ values in pyrite from the massive sulfide and chlorite-quartz-chalcopyrite-pyrite zones of the Ashele VMS deposit.

system. Episodic releases of metalliferous magmatic fluids have been well documented in several types of magmatic-hydrothermal systems, including porphyry, skarn, and vein-type Sn-W deposits, and have been suggested to be critically important for metal enrichment (Li et al. 2017, 2018, 2022a, 2022b). We suggest that episodic inputs of magmatic volatiles are also critical for accumulating metals at Ashele. In addition to Cu, As, Te, Se, Sb, Pb, Tl, and Hg, the episodic inputs of magmatic volatiles also cause significant increases in Mn, Zn, and Mo concentrations (Online Materials[1] Appendix VI).

Differing from the scenario in the massive sulfide zone, the positive $\delta^{34}S$ values of growth zones in pyrite from the chlorite-quartz-chalcopyrite-pyrite zones with abnormally high Cu and As contents cannot be explained by the input of magmatic volatiles alone. These growth zones display porous textures with low contents of volatile elements (Hg and Tl), indicating rapid crystallization during vigorous boiling, an efficient process for the precipitation of Cu from hydrothermal fluids due to the destabilization of Cu complexes (Román et al. 2019). Previous studies suggested that hydrothermal fluid boiling in low-pressure environments would result in the separation of liquid and vapor phases (Román et al. 2019; Falkenberg et al. 2022). Pyrite formed under such conditions of fluid boiling is usually characterized by porous textures with abundant mineral inclusions (Online Materials[1] Appendix IVa), relatively high As, Cu, Pb, and Ag but low Hg, Tl, and Ni concentrations (Online Materials[1] Appendix V) (Román et al. 2019). In addition, fluid inclusion analyses of Yang et al. (2018) also provided compelling evidence for fluid boiling that had taken place in the chlorite-quartz-chalcopyrite-pyrite zone. It is also important to note that at least three fluid boiling events were recorded in a single pyrite grain from the chlorite-quartz-chalcopyrite-pyrite zone (Fig. 4; Online Materials[1] Appendix IV), suggesting that fluid boiling may have played a crucial role in the formation of the stringer-zone orebody in the Ashele deposit. In addition, similar $\delta^{34}S$ values from Cu-rich and Cu-poor pyrite growth zones in the chlorite-quartz-chalcopyrite-pyrite zone (Online Materials[1] Appendix IVa) argue for insignificant S isotopic fractionation between the liquid and vapor phases during fluid boiling.

Controls of sub-seafloor Cu mineralization

The abnormally high Cu concentrations of certain growth zones in pyrite from the Ashele deposit (>1 wt%; Figs. 3 and 4) indicate that this mineral may have acted as an important Cu scavenger in VMS deposits, similar to that documented in porphyry-epithermal hydrothermal deposits (Pačevski et al. 2008; Deditius et al. 2009; Reich et al. 2013). The alternating occurrences of Cu-rich and Cu-poor growth zones within single pyrite grains in both the massive sulfide and chlorite-sulfide zones suggest that Cu mineralization at the Ashele VMS deposit was not a continuous process but rather episodic. Such abrupt and rhythmic changes in the composition of the pyrite-forming fluids are likely related to changes in physicochemical conditions due to multi-stage fluid boiling and episodic inputs of magmatic volatiles. This complex evolution of fluids in the Ashele VMS deposit was probably related to pulses of magmatic activity from the underlying magma chamber in a similar fashion to those observed in porphyry, skarn, and vein-type Sn-W deposits (Li et al. 2017, 2018, 2022a, 2022b).

These results suggest that the Ashele VMS deposit formed in a magmatic-hydrothermal system characterized by at least two pulses of magmatic fluids, which provided both the heat sources and ore-forming materials. In addition, fluid boiling and input of magmatic volatiles operated in different zones of the Ashele deposit that might be related to the different locations of the massive sulfide and chlorite-quartz-chalcopyrite-pyrite zones. The massive sulfide zone is usually situated at the top of VMS deposits, where volatiles can easily reach. In contrast, the chlorite-quartz-chalcopyrite-pyrite zone is located in the lower and outer parts of VMS deposits where magmatic fluids could mix with seawater and cause boiling (Fig. 6). In summary, in situ SIMS sulfur isotopic analysis and LA-ICP-MS element mapping of texturally distinct pyrite indicates multi-stage fluid boiling and episodic inputs of magmatic volatiles occurred in the Ashele VMS deposit. Moreover, our results suggest that such episodic magmatic activities from the underlying magmatic systems (Fig. 6) could be the essential prerequisite to forming large-tonnage VMS deposits.

Implications

Previous studies of modern VMS systems have suggested that magmatic fluids from the underlying magma chamber contribute ore-forming metals to VMS-hydrothermal systems (Yang and Scott 1996; de Ronde et al. 2011; Brueckner et al. 2014; Martin et al. 2020; Falkenberg et al. 2022). However, the question of whether magmatic fluids play an important role in the mineralization processes of ancient VMS deposits remains unclear because they have often been variably overprinted by later tectonic and deformation events. Our detailed documentation of pyrite textures combined with systematic in situ SIMS sulfur isotope analyses and LA-ICP-MS elemental mapping of zoned pyrite grains, provide significant new insights into the source and evolution of the ore-forming fluids in the Early to Middle Devonian Ashele VMS deposit. Highly variable $\delta^{34}S$ values and elemental compositions of pyrite grains at the intragrain scale reveal multi-stage fluid boiling or episodic inputs of magmatic volatiles, which resulted in abnormally high Cu-As contents in pyrite. The occurrence of alternating Cu-rich and Cu-poor growth zones in pyrite suggests that Cu mineralization of the Ashele VMS deposit is episodic rather than continuous. This study shows that integrating detailed textural observations with in situ sulfur isotopic and trace-element analyses of pyrite can be used to document and distinguish fluid boiling and episodic inputs of magmatic volatiles, which may be important processes to form large-tonnage VMS deposits. It is also interesting to note that we documented distinct textural patterns and contrasting trace-element compositions and sulfur isotopic signatures in pyrite between the massive sulfide zone and chlorite-quartz-chalcopyrite-pyrite zones in the Ashele deposit. These differences are interpreted to record different processes operating in different parts of VMS systems. Therefore, a comprehensive understanding of mineralization processes in VMS deposits requires a systematic study of pyrite from all parts of individual deposits.

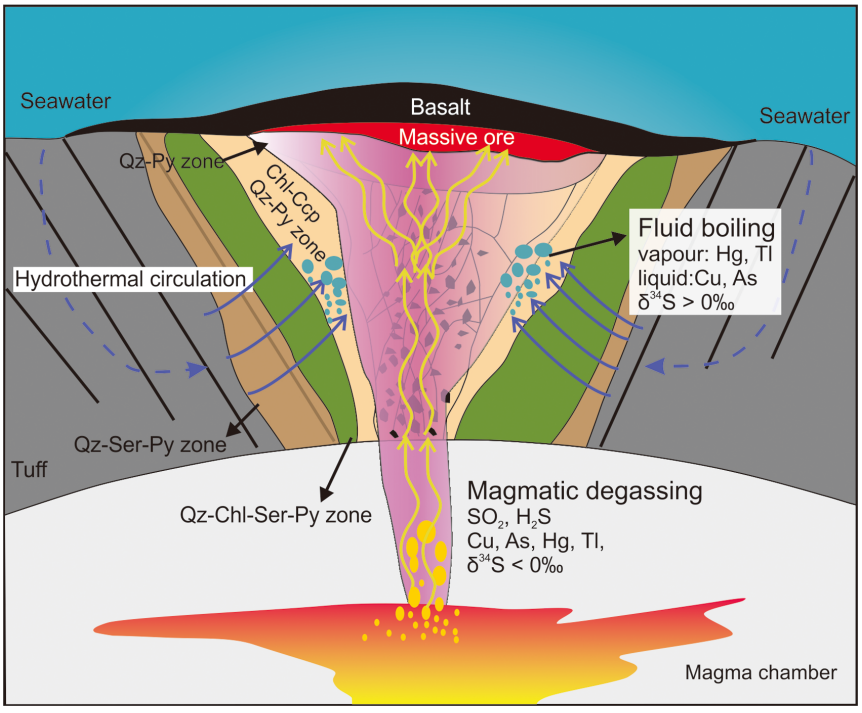

Figure 6. Schematic model of the Ashele Cu-Zn deposit (not true to scale) showing the evolution of the magmatic-hydrothermal system. Evidence of fluid boiling and episodic inputs of magmatic volatiles is provided by in situ SIMS sulfur isotopes and elemental mapping of texturally distinct pyrite. (Color online.)

Finally, Fox et al. (2020) also investigated zoned epidote in an alteration pipe of the Troodos ophiolite to track magmatic fluids and used it to show episodic fluxing of magmatic fluids in oceanic hydrothermal systems. Hypothetically, all ore- and rock-forming minerals such as quartz (e.g., Götze et al. 2021) in VMS deposits are potential tracers for deciphering mineralization processes and related magmatic-hydrothermal activities. In practice, many minerals of low abundance and/or narrow stability fields often have restricted occurrences and limited paragenesis in VMS systems, thus making them less useful as tracers. For example, BSE imaging combined with in situ SIMS analyses of chalcopyrite and sphalerite (Yang et al. 2018; Xiao et al. 2024), including those after NaOCl etching, showed that these two minerals in the Ashele deposit are texturally and compositionally uniform within individual grains and have limited variations in general, thus representing poor tracers of the complex, episodic magmatic-hydrothermal activities. Two obvious advantages of pyrite over most other minerals are: (1) its ubiquitous occurrence, local high abundances, and close spatial-temporal associations with mineralization in VMS deposits and (2) its complex, pronounced, and robust textural and chemical variations that are readily documented by modern analytical techniques. Therefore, the linkage between textural and geochemical features of zoned pyrite established in the Ashele deposit and ore-forming processes (such as fluid boiling and magmatic volatile influx) can be applied to reveal mineralization processes in ancient VMS deposits worldwide and may also constitute a significant exploration guide for VMS ores.

Acknowledgments and Funding

This study was funded by the National Key R&D Program of China (2022YFC2903301), the Xinjiang Key Research and Development Program (2023B03014), the National Natural Science Foundation of China (42173065, 42230810, 41921003, U2344208), the CAS Project for Young Scientists in Basic Research (YSBR-082), Science and Technology Planning Project of Guangdong Province (2023B1212060048), and Applied Basic Research Subject (Young Doctor "Sailing" project) (2024A04J4749). Yuzhou Feng is partially supported by an NSERC-CREATE INSPIRE postdoctoral fellowship. The manuscript benefited from constructive reviews by Yang Li, Roberge, Gregory, Brueckner, Reynolds, and two anonymous referees, which we greatly appreciate.

References Cited

Barrie, C.T., Cathles, L.M., and Erendi, A. (1999) Finite element heat and fluid-flow computer simulations of a deep ultramafic sill model for the Giant Kidd Creek volcanic-associated massive sulfide deposit, Abitibi Subprovince, Canada. Economic Geology Monographs, 10, 529–540.

Berkenbosch, H.A., de Ronde, C.E.J., Ryan, C.G., McNeill, A.W., Howard, D.L., Gemmell, J.B., and Danyushevsky, L.V. (2019) Trace element mapping of copper- and zinc-rich black smoker chimneys from Brothers Volcano, Kermadec Arc, using synchrotron radiation XFM and LA-ICP-MS. Economic Geology and the Bulletin of the Society of Economic Geologists, 114, 67–92, https://doi.org/10.5382/econgeo.2019.4620.

Brueckner, S.M., Piercey, S.J., Sylvester, P.J., Maloney, S., and Pilgrim, L. (2014) Evidence for syngenetic precious metal enrichment in an Appalachian Volcanogenic Massive Sulfide System: The 1806 Zone, Ming Mine, Newfoundland, Canada. Economic Geology and the Bulletin of the Society of Economic Geologists, 109, 1611–1642, https://doi.org/10.2113/econgeo.109.6.1611.

Brueckner, S.M., Piercey, S.J., Layne, G.D., Piercey, G., and Sylvester, P.J. (2015) Variations of sulphur isotope signatures in sulphides from the metamorphosed Ming Cu(-Au) volcanogenic massive sulphide deposit, Newfoundland Appalachians, Canada. Mineralium Deposita, 50, 619–640, https://doi.org/10.1007/s00126-014-0567-7.

Brueckner, S.M., Piercey, S.J., Pilote, J.-L., Layne, G.D., and Sylvester, P.J. (2016) Mineralogy and mineral chemistry of the metamorphosed and precious metal-bearing Ming deposit, Canada. Ore Geology Reviews, 72, 914–939, https://doi.org/10.1016/j.oregeorev.2015.09.016.

Cathles, L.M. (1983) An analysis of the hydrothermal system responsible for massive sulfide deposition in the Hokuroku Basin of Japan. Economic Geology Monographs, 5, 439–487, https://doi.org/10.5382/Mono.05.27.

de Ronde, C.E.J., Massoth, G.J., Butterfield, D.A., Christenson, B.W., Ishibashi, J., Ditchburn, R.G., Hannington, M.D., Brathwaite, R.L., Lupton, J.E., Kamenetsky, V.S., and others. (2011) Submarine hydrothermal activity and gold-rich mineralization at Brothers Volcano, Kermadec Arc, New Zealand. Mineralium Deposita, 46, 541–584, https://doi.org/10.1007/s00126-011-0345-8.

Deditius, A.P., Utsunomiya, S., Ewing, R.C., Chryssoulis, S.L., Venter, D., and Kesler, S.E. (2009) Decoupled geochemical behavior of As and Cu in hydrothermal systems. Geology, 37, 707–710, https://doi.org/10.1130/G25781A.1.

Falkenberg, J.J., Keith, M., Haase, K.M., Bach, W., Klemd, R., Strauss, H., Yeo, I.A., Rubin, K.H., Storch, B., and Anderson, M.O. (2021) Effects of fluid boiling on Au and volatile element enrichment in submarine arc-related hydrothermal systems. Geochimica et Cosmochimica Acta, 307, 105–132, https://doi.org/10.1016/j.gca.2021.05.047.

Falkenberg, J.J., Keith, M., Haase, K.M., Sporer, C., Bach, W., Klemd, R., Strauss, H., Storch, B., Peters, C., Rubin, K.H., and Anderson, M.O. (2022) Spatial variations in magmatic volatile influx and fluid boiling in the submarine hydrothermal systems of Niuatahi Caldera, Tonga Rear-Arc. Geochemistry, Geophysics, Geosystems, 23, e2021GC010259.

Fox, S., Katzir, Y., Bach, W., Schlicht, L., and Glessner, J. (2020) Magmatic volatiles episodically flush oceanic hydrothermal systems as recorded by zoned epidote. Communications Earth & Environment, 1, 52, https://doi.org/10.1038/s43247-020-00051-0.

Franklin, J.M., Gibson, H.L., Jonasson, I.R., and Galley, A.G. (2005) Volcanogenic massive sulfide deposits. Economic Geology 100th anniversary volume, 98, 523–560.

Gilbert, S.E., Danyushevsky, L.V., Rodemann, T., Shimizu, N., Gurenko, A., Meffre, S., Thomas, H., Large, R.R., and Death, D. (2014) Optimisation of laser parameters for the analysis of sulphur isotopes in sulphide minerals by laser ablation ICP-MS. Journal of Analytical Atomic Spectrometry, 29, 1042–1051, https://doi.org/10.1039/C4JA00011K.

Götze, J., Pan, Y.M., and Müller, A. (2021) Mineralogy and mineral chemistry of quartz: A review. Mineralogical Magazine, 85, 639–664, https://doi.org/10.1180/mgm.2021.72.

Hannington, M.D. (2014) Volcanogenic massive sulfide deposits. In S.D. Scott, Ed., Treatise on Geochemistry, 2nd ed., 13, 463–488. Elsevier Science.

Herzig, P.M., Hannington, M.D., and Arribas, A. Jr. (1998) Sulfur isotopic composition of hydrothermal precipitates from the Lau back-arc: Implications for magmatic contributions to seafloor hydrothermal systems. Mineralium Deposita, 33, 226–237, https://doi.org/10.1007/s001260050143.

Holser, W.T. (1977) Catastrophic chemical events in the history of the ocean. Nature, 267, 403–408, https://doi.org/10.1038/267403a0.

Ishida, M., Romero, R., Leisen, M., Yasukawa, K., Nakamura, K., Barra, F., Reich, M., and Kato, Y. (2022) Auriferous pyrite formed by episodic fluid inputs in the Akeshi and Kasuga high-sulfidation deposits, Southern Kyushu, Japan. Mineralium Deposita, 57, 129–145, https://doi.org/10.1007/s00126-021-01053-4.

Jowitt, S.M., Jenkin, G.R.T., Coogan, L.A., and Naden, J. (2012) Quantifying the release of base metals from source rocks for volcanogenic massive sulfide deposits: Effects of protolith composition and alteration mineralogy. Journal of Geochemical Exploration, 118, 47–59, https://doi.org/10.1016/j.gexplo.2012.04.005.

Keith, M., Haase, K.M., Chivas, A.R., and Klemd, R. (2022) Phase separation and fluid mixing revealed by trace element signatures in pyrite from porphyry systems. Geochimica et Cosmochimica Acta, 329, 185–205, https://doi.org/10.1016/j.gca.2022.05.015.

Large, R.R. (1992) Australian volcanic-hosted massive sulfide deposits; features, styles, and genetic models. Economic Geology and the Bulletin of the Society of Economic Geologists, 87, 471–510, https://doi.org/10.2113/gsecongeo.87.3.471.

Large, R.R., Danyushevsky, L., Hollit, C., Maslennikov, V., Meffre, S., Gilbert, S., Bull, S., Scott, R., Emsbo, P., Thomas, H., and others. (2009) Gold and trace element zonation in pyrite using a laser imaging technique: Implications for the timing of gold in orogenic and Carlin-Style Sediment-Hosted Deposits. Economic Geology and the Bulletin of the Society of Economic Geologists, 104, 635–668, https://doi.org/10.2113/gsecongeo.104.5.635.

Layton-Matthews, D., Leybourne, M.I., Peter, J.M., Scott, S.D., Cousens, B., and Eglington, B.M. (2013) Multiple sources of selenium in ancient seafloor hydrothermal systems: Compositional and Se, S, and Pb isotopic evidence from volcanic-hosted and volcanic-sediment-hosted massive sulfide deposits of the Finlayson Lake District, Yukon, Canada. Geochimica et Cosmochimica Acta, 117, 313–331, https://doi.org/10.1016/j.gca.2013.05.002.

Li, Y., Selby, D., Condon, D., and Tapster, S. (2017) Cyclic magmatic-hydrothermal evolution in porphyry systems: High-precision U-Pb and Re-Os geochronology constraints on the Tibetan Qulong Porphyry Cu-Mo Deposit. Economic Geology and the Bulletin of the Society of Economic Geologists, 112, 1419–1440, https://doi.org/10.5382/econgeo.2017.4515.

Li, Y., Li, X.H., Selby, D., and Li, J.W. (2018) Pulsed magmatic fluid release for the formation of porphyry deposits: Tracing fluid evolution in absolute time from the Tibetan Qulong Cu-Mo deposit. Geology, 46, 7–10, https://doi.org/10.1130/G39504.1.

Li, R.C., Chen, H.Y., Large, R.R., Zhao, L.D., Liu, Y.H., Jiao, J.G., Xia, X.P., and Yang, Q. (2020) Ore-forming fluid source of the orogenic gold deposit: Implications from a combined pyrite texture and geochemistry study. Chemical Geology, 552, 119781, https://doi.org/10.1016/j.chemgeo.2020.119781.

Li, Y., Allen, M.B., and Li, X.H. (2022a) Millennial pulses of ore formation and an extra-high Tibetan Plateau. Geology, 50, 665–669, https://doi.org/10.1130/G49911.1.

Li, Y., Zhang, R.Q., He, S., Chiaradia, M., and Li, X.H. (2022b) Pulsed exsolution of magmatic ore-forming fluids in tin-tungsten systems: A SIMS cassiterite oxygen isotope record. Mineralium Deposita, 57, 343–352, https://doi.org/10.1007/s00126-022-01093-4.

Maier, W.D., Smithies, R.H., Spaggiari, C.V., Barnes, S.J., Kirkland, C.L., Yang, S., Lahaye, Y., Kiddie, O., and MacRae, C. (2016) Petrogenesis and Ni-Cu sulphide potential of mafic–ultramafic rocks in the Mesoproterozoic Fraser Zone within the Albany-Fraser Orogen, Western Australia. Precambrian Research, 281, 27–46, https://doi.org/10.1016/j.precamres.2016.05.004.

Martin, A.J., Keith, M., Parvaz, D.B., McDonald, I., Boyce, A.J., McFall, K.A., Jenkin, G.R.T., Strauss, H., and MacLeod, C.J. (2020) Effects of magmatic volatile influx in mafic VMS hydrothermal systems: Evidence from the Troodos ophiolite, Cyprus. Chemical Geology, 531, 119325, https://doi.org/10.1016/j.chemgeo.2019.119325.

Molnár, F., Mänttäri, I., O'Brien, H., Lahaye, Y., Pakkanen, L., Johanson, B., Käpyaho, A., Sorjonen-Ward, P., Whitehouse, M., and Sakellaris, G. (2016) Boron, sulphur and copper isotope systematics in the orogenic gold deposits of the Archaean Hattu schist belt, eastern Finland. Ore Geology Reviews, 77, 133–162, https://doi.org/10.1016/j.oregeorev.2016.02.012.

Nozaki, T., Nagase, T., Ushikubo, T., Shimizu, K., Ishibashi, J.-i., and the D/V Chikyu Expedition 909 Scientists (2020) Microbial sulfate reduction plays an important role at the initial stage of subseafloor sulfide mineralization. Geology, 49, 222–227, https://doi.org/10.1130/G47943.1.

Ohmoto, H. (1972) Systematics of sulfur and carbon isotopes in hydrothermal ore deposits. Economic Geology and the Bulletin of the Society of Economic Geologists, 67, 551–578, https://doi.org/10.2113/gsecongeo.67.5.551.

Pačevski, A., Libowitzky, E., Živković, P., Dimitrijević, R., and Cvetković, L. (2008) Copper-bearing pyrite from the Čoka Marin polymetallic deposit, Serbia: Mineral inclusions or true solid-solution? Canadian Mineralogist, 46, 249–261, https://doi.org/10.3749/canmin.46.1.249.

Paton, C., Hellstrom, J., Paul, B., Woodhead, J., and Hergt, J. (2011). Iolite: Freeware for the visualisation and processing of mass spectrometric data, 26, 2508–2518.

Patten, C.G.C., Pitcairn, I.K., and Teagle, D.A.H. (2017) Hydrothermal mobilisation of Au and other metals in supra-subduction oceanic crust: Insights from the Troodos ophiolite. Ore Geology Reviews, 86, 487–508, https://doi.org/10.1016/j.oregeorev.2017.02.019.

Reich, M., Deditius, A., Chryssoulis, S., Li, J.W., Ma, C.Q., Parada, M.A., Barra, F., and Mittermayr, F. (2013) Pyrite as a record of hydrothermal fluid evolution in a porphyry copper system: A SIMS/EMPA trace element study. Geochimica et Cosmochimica Acta, 104, 42–62, https://doi.org/10.1016/j.gca.2012.11.006.

Richardson, C.J., Cann, J.R., Richards, H.G., and Cowan, J.G. (1987) Metal-depleted root zones of the Troodos ore-forming hydrothermal systems, Cyprus. Earth and Planetary Science Letters, 84, 243–253, https://doi.org/10.1016/0012-821X(87)90089-6.

Román, N., Reich, M., Leisen, M., Morata, D., Barra, F., and Deditius, A.P. (2019) Geochemical and micro-textural fingerprints of boiling in pyrite. Geochimica et Cosmochimica Acta, 246, 60–85, https://doi.org/10.1016/j.gca.2018.11.034.

Schardt, C. and Large, R.R. (2009) New insights into the genesis of volcanic-hosted massive sulfide deposits on the seafloor from numerical modeling studies. Ore Geology Reviews, 35, 333–351, https://doi.org/10.1016/j.oregeorev.2008.11.008.

Seyfried, W.E., Jr. and Ding, K. (1993) The effect of redox on the relative solubilities of copper and iron in Cl-bearing aqueous fluids at elevated temperatures and pressures: An experimental study with application to subseafloor hydrothermal systems. Geochimica et Cosmochimica Acta, 57, 1905–1917, https://doi.org/10.1016/0016-7037(93)90083-9.

Tardani, D., Reich, M., Deditius, A.P., Chryssoulis, S., Sánchez-Alfaro, P., Wrage, J., and Roberts, M.P. (2017) Copper–arsenic decoupling in an active geothermal system: A link between pyrite and fluid composition. Geochimica et Cosmochimica Acta, 204, 179–204, https://doi.org/10.1016/j.gca.2017.01.044.

Wan, B., Zhang, L.C., and Xiang, P. (2010) The Ashele VMS-type Cu-Zn Deposit in Xinjiang, NW China formed in a rifted arc setting. Resource Geology, 60, 150–164, https://doi.org/10.1111/j.1751-3928.2010.00122.x.

Wohlgemuth-Ueberwasser, C.C., Viljoen, F., Petersen, S., and Vorster, C. (2015) Distribution and solubility limits of trace elements in hydrothermal black smoker sulfides: An in-situ LA-ICP-MS study. Geochimica et Cosmochimica Acta, 159, 16–41, https://doi.org/10.1016/j.gca.2015.03.020.

Xiao, B., Chen, H.Y., Huang, F., Feng, Y.Z., Hu, X., and Li, R.C. (2024) Iron, boron, and sulfur isotope constraints on the ore-forming process of subseafloor replacement-style volcanogenic massive sulfide systems. Geological Society of America Bulletin, 136, 1037–1049.

Yang, K.H. and Scott, S.D. (1996) Possible contribution of a metal-rich magmatic fluid to a sea-floor hydrothermal system. Nature, 383, 420–423, https://doi.org/10.1038/383420a0.

Yang, F.Q., Li, Q., Yang, C.D., and Zhang, Z.X. (2018) A combined fluid inclusion and S-H-O-He-Ar isotope study of the Devonian Ashele VMS-type copper-zinc

deposit in the Altay orogenic belt, northwest China. Journal of Asian Earth Sciences, 161, 139–163, https://doi.org/10.1016/j.jseaes.2018.05.012.
Zhang, Y., Chen, H.Y., Cheng, J.M., Tian, J., Zhang, L.J., and Olin, P. (2022) Pyrite geochemistry and its implications on Au-Cu skarn metallogeny: An example from the Jiguanzui deposit. American Mineralogist, 107, 1910–1925, https://doi.org/10.2138/am-2022-8118.
Zheng, Y., Wang, Y.J., Chen, H.Y., Lin, Z.W., Hou, W.S., and Li, D.F. (2016) Micro-textural and fluid inclusion data constraints on metallic remobilization of the Ashele VMS Cu-Zn deposit, Altay, NW China. Journal of Geochemical Exploration, 171, 113–123, https://doi.org/10.1016/j.gexplo.2016.06.015.

Manuscript received November 12, 2023
Manuscript accepted August 29, 2024
Accepted manuscript online September 3, 2024
Manuscript Handled by Julie Roberge

Endnotes:

[1]Deposit item AM-25-59250. Online Materials are free to all readers. Go online, via the table of contents or article view, and find the tab or link for supplemental materials.